Low density solid ozone

ARTICLE *in* THE JOURNAL OF CHEMICAL PHYSICS · SEPTEMBER 2007

Impact Factor: 2.95 · DOI: 10.1063/1.2762215 · Source: PubMed

3 AUTHORS:

Ben Teolis
Southwest Research Institute
84 PUBLICATIONS **659** CITATIONS
SEE PROFILE

M. Famá
University of Virginia
53 PUBLICATIONS **461** CITATIONS
SEE PROFILE

Raul A. Baragiola
University of Virginia
406 PUBLICATIONS **4,900** CITATIONS
SEE PROFILE

Low density solid ozone

B. D. Teolis, M. Famá, and R. A. Baragiola[a)]
Laboratory for Atomic and Surface Physics, University of Virginia, Charlottesville, Virginia 22904, USA

(Received 5 April 2007; accepted 27 June 2007; published online 21 August 2007)

We report a very low density ($\sim$0.5 g/cm^3) structure of solid ozone. It is produced by irradiation of solid oxygen with 100 keV protons at 20 K followed by heating to sublime unconverted oxygen. Upon heating to 47 K the porous ozone compacts to a density of $\sim$1.6 g/cm^3 and crystallizes. We use a detailed analysis of the main infrared absorption band of the porous ozone to interpret previous research, where solid oxygen was irradiated by UV light and keV electrons. © *2007 American Institute of Physics*. [DOI: 10.1063/1.2762215]

INTRODUCTION

The presence of condensed ozone in nature was inferred a decade ago from the detection of ultraviolet absorption in the reflectance spectra of Ganymede,[1] Rhea, and Dione.[2] The surface of these satellites is predominantly covered by water ice, and thus it was proposed that ozone is a by-product of radiolysis of ice by energetic particles, trapped in the magnetospheres of Jupiter and Saturn. The process would start with the dissociation of water molecules, formation and trapping of O_2, and the radiosynthesis of O_3 from O_2.[2] Laboratory experiments have shown the production of ozone by energetic electron and ion bombardment of condensed oxygen,[3–5] and we have recently discussed the conditions to form sufficient amounts of precursor O_2 in water ice for ozone synthesis.[6]

Astronomical observations and laboratory experiments have used the Hartley absorption band of ozone for its identification. This broad absorption at 254 nm in atmospheric ozone shields life on Earth from the harmful influence of solar ultraviolet radiation.[7] Potentially more detailed information is available from the narrow ν_3 and $\nu_1+\nu_3$ bands in the infrared near 1043 and 2108 cm^{-1} corresponding to the O–O asymmetric stretch vibrational mode and the symmetric-asymmetric stretch combination mode. These infrared bands have been used to characterize matrix-isolated O_3 (Refs. 8–14) and to interpret the environment of ozone molecules deposited from the vapor or produced by photolysis[15,16] and radiolysis of solid O_2.[17] Here we report on laboratory studies of the production of ozone by irradiating solid O_2 with 100 keV protons, with the aim of exploring the physical characteristics of the ozone residue produced on warming. The results of a detailed analysis of optical reflectance in the ultraviolet and infrared show the existence of a previously unknown low density phase of solid ozone ($\sim$0.5 g/cm^3) and throw light on the interpretation of previous infrared absorption experiments.

EXPERIMENTS

We performed all experiments in a cryopumped, ultrahigh vacuum chamber with an ultimate pressure of 3 $\times 10^{-10}$ Torr. Films containing 1000 ML of O_2 (1 ML $\sim 10^{15}$ molecules cm^{-2} or approximately a monolayer on a surface) were vapor deposited at $\sim$10–20 K from a microcapillary doser onto a liquid helium cooled gold-coated quartz-crystal microbalance, which measures the areal mass Q (mass/unit area) deposited with a sensitivity of $\sim$0.1 ML. We irradiated the films with 100 keV protons to a fluence of $\sim 3\times 10^{14}$ cm^{-2}, which is sufficient to saturate the concentration of ozone produced.[4,5] After preparation of the films, we warmed them at $\sim$0.15 K min^{-1} while monitoring their specular reflectance in the infrared (650–9000 cm^{-1}) and ultraviolet-visible (230–850 nm) regions of the spectrum. The infrared and UV-visible reflectance spectra were measured with unpolarized light at 35° and 4° angles of incidence, respectively. From $\boldsymbol{R}/\boldsymbol{R}_0$, the ratio of the reflectance of the sample to that of the bare substrate, we derive the optical depth, $-\ln(\boldsymbol{R}/\boldsymbol{R}_0)$, and the integrated band area B_T, in terms of the wavelength λ of the light,

$$B_T = -\int \ln(\boldsymbol{R}/\boldsymbol{R}_0)d(1/\lambda). \quad (1)$$

From the reflectance, we calculated the refraction index, absorbance, and thickness of the films. The density of the films was then deduced from the ratio of mass per unit area to thickness.

ANALYSIS OF THE REFLECTANCE SPECTRA

We derive the O_3 column density η from the UV reflectance of the film using the absorption cross section at the maximum of the Hartley band, which has been measured in the gas phase to be $\sim 1.1\times 10^{-17}$ cm^2.[18] In the case of a gas, the absorption cross section σ is related to the absorbance A via

$$A = \sigma N, \quad (2)$$

where N is the density of absorbing molecules and A determines the decay of the light intensity along the direction of propagation by Beer's law: $I=I_0e^{-Ax}$, where x is the propagation distance. In contrast to a gas, the polarization of dense materials is enhanced because the polarizing field on each molecule is augmented by the polarization of the neighboring molecules, which increases the ability of the material to

a)Author to whom correspondence should be addressed. Electronic mail: raul@virginia.edu

absorb energy. Therefore, Eq. (2) underestimates the absorbance at solid state densities. A more accurate way of relating the optical properties of a solid to the number of absorbing molecules is the Lorentz-Lorenz or Clausius-Mosotti equation,[19]

$$\frac{3}{4\pi}\frac{\boldsymbol{n}^2-1}{\boldsymbol{n}^2+2}=\sum_j \alpha_j N_j, \tag{3}$$

where N_j and α_j are number densities of molecules and molecular polarizabilities of different species in the solid, respectively, and $\boldsymbol{n}$, the complex index of refraction of the material, is related to the absorbance through its imaginary component,

$$\boldsymbol{n}=n-ik=n-i\frac{\lambda}{4\pi}A, \tag{4}$$

where λ is the wavelength of the light incident onto the solid. Using Eqs. (3) and (4) to express A in terms of N_j and α_j, we obtain

$$A=-\frac{4\pi}{\lambda}\,\mathrm{Im}\sqrt{\frac{8\pi\Sigma_j\alpha_j N_j+3}{3-4\pi\Sigma_j\alpha_j N_j}}. \tag{5}$$

We now expand Eq. (5) to first order with respect to the density N_m of an absorbing species m in the solid,

$$\begin{aligned}A(N_m)&=\sum_i \frac{1}{l!}\frac{d^l A(0)}{dN_m^l}N_m^l\\&=-\frac{72\pi^2}{\lambda}\,\mathrm{Im}\left[\alpha_m\left(\frac{9}{3-4\pi\Sigma_{j\neq m}\alpha_j N_j}-2\right)^{-1/2}\right.\\&\left.\times\left(3-4\pi\sum_{j\neq m}\alpha_j N_j\right)^{-2}\right]N_m+\ \ldots\ +\ .\end{aligned} \tag{6}$$

In the gas phase, N_m is sufficiently small that terms higher than the first order can be dropped, and Eqs. (6) and (2) are equivalent. Comparison of these equations yields an expression for the gas phase absorption cross section for molecules of species m,

$$\begin{aligned}\sigma=-\frac{72\pi^2}{\lambda}\,\mathrm{Im}&\left[\alpha_m\left(\frac{9}{3-4\pi\Sigma_{j\neq m}\alpha_j N_j}-2\right)^{-1/2}\right.\\&\left.\times\left(3-4\pi\sum_{j\neq m}\alpha_j N_j\right)^{-2}\right].\end{aligned} \tag{7}$$

For pure ozone, $\Sigma_{j\neq m}\alpha_j N_j=0$, and the above becomes

$$\sigma_{O_3}=-\frac{8\pi^2\,\mathrm{Im}(\alpha_{O_3})}{\lambda}, \tag{8}$$

where α_{O_3} is the molecular polarizability of O_3 and $\sigma_{O_3}=1.1\times10^{-17}$ cm^2 is the gas phase absorption cross section of the O_3 molecule. For experiments where condensed O_3 is mixed with solid O_2, α_{O_3} can be expressed in terms of the complex index $\boldsymbol{n}$ of the mixture by way of Eq. (3),

$$\alpha_{O_3}=\frac{1}{N_{O_3}}\left(\frac{3}{4\pi}\frac{\boldsymbol{n}^2-1}{\boldsymbol{n}^2+2}-\alpha_{O_2}N_{O_2}\right), \tag{9}$$

where α_{O_2} and N_{O_2} are the polarizability and the density of O_2 molecules. Finally, taking α_{O_2} to be a real number (since O_2 does not absorb in the wavelength range of the ozone Hartley band) and substituting Eq. (9) into Eq. (8), we can solve for the ozone column density $\eta=N_{O_3}z$ in an O_2:O_3 film of thickness z, yielding

$$\eta=N_{O_3}z=\frac{-6\pi z}{\lambda\sigma_{O_3}}\,\mathrm{Im}\left(\frac{\boldsymbol{n}^2-1}{\boldsymbol{n}^2+2}\right). \tag{10}$$

We point out that N_{O_2} in Eq. (9) is equal to $(Q-\eta M_{O_3})/zM_{O_2}$, where M_{O_2} and M_{O_3} are the O_2 and O_3 molecule masses, respectively.

We determine $\boldsymbol{n}$ and z by a fit of the exact expression for the reflectance $\boldsymbol{R}$ of a thin film divided by that of the substrate, $\boldsymbol{R}_0=(|r_{s0}^S|^2+|r_{s0}^P|^2)/2$,[20,21]

$$\begin{aligned}\frac{\boldsymbol{R}}{\boldsymbol{R}_0}=\frac{1}{(|r_{2s0}|^2+|r_{2p0}|^2)}&\left(\left|\frac{r_{1s}+r_{2s}e^{-2i\delta}}{1+r_{1s}r_{2s}e^{-2i\delta}}\right|^2\right.\\&\left.+\left|\frac{r_{1p}+r_{2p}e^{-2i\delta}}{1+r_{1p}r_{2p}e^{-2i\delta}}\right|^2\right),\end{aligned} \tag{11}$$

to the measured reflectance spectrum. Here, the phase shift $\delta=2\pi\boldsymbol{n}z\cos\varphi/\lambda$, r_{1s}, r_{1p}, r_{2s}, and r_{2p} are the Fresnel reflection coefficients of the film and substrate surfaces at s and p polarizations, and the angle of refraction φ of the light in the film is calculated from $\boldsymbol{n}$ using Snell's law. The fit is constrained by the Kramers-Kronig dispersion relations[22–25] between the real and imaginary parts of $\boldsymbol{n}$.

For strong absorption such as in the Hartley and ν_3 bands of solid ozone, optical interference generates intense distortions in the appearance of the band when measured in reflectance, a phenomenon mostly due to the strong variation of n across the band. To illustrate this effect, we consider a model film with the absorbance A and refraction index with real part n depicted in Fig. 1(a), where $A(\lambda)$ is a Gaussian centered at 1040 cm^{-1} to simulate an absorption band. In Fig. 1(b), we calculate from Eq. (11) the optical depth of films of different thicknesses on a gold substrate measured at 35° incidence with unpolarized light. At a fixed wavelength, the optical depth generally increases with film thickness but also oscillates in response to cycles of destructive and constructive interference. The cycles become more rapid as one moves across the absorption band toward longer wavelengths where n is greatest, producing a complicated evolution in the shape and location of bands in the optical depth spectrum. The appearance of a second peak at nonnormal incidence [Fig. 1(c)] is mostly due to the p-polarized component of the incident light, a phenomenon first described by Berreman.[26] If these optical interference effects are not considered, one may misinterpret the appearance of satellites or shoulders in absorption bands. Hence, the optical properties of the film are more realistically characterized by $\boldsymbol{n}$ (i.e., n and A) or α rather than by the optical depth measured in reflectance.

We note that in the literature one can often find that an erroneous expression is used to calculate the column density

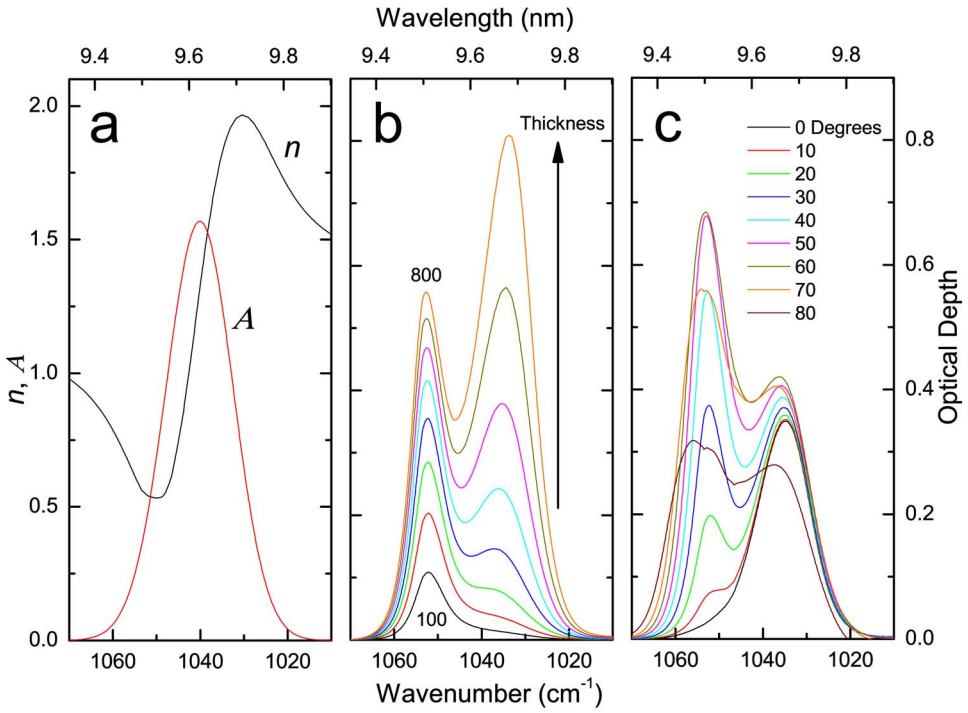

FIG. 1. (a) The real part n of the refraction index and the absorbance A (in units of μm^{-1}) within an absorption band of a model material. $A(\lambda)$ is chosen to be a Gaussian centered at 1040 cm^{-1}, and n and A satisfy the Kramers-Kronig dispersion relations. (b) The optical depth, $-\ln(R/R_0)$, of films of different thicknesses on a gold substrate calculated from Eq. (11) using the optical constants of (a) and an incidence angle of 35°. Thicknesses range from 100 to 800 nm in increments of 100 nm. (c) $-\ln(R/R_0)$ at different angles of incidence for a 600 nm thick film on a gold substrate calculated from Eq. (11) using the optical constants of (a).

η of an absorbing species from the integrated area of an absorption band: $\eta = -(\cos\varphi/2A)\int_{\lambda_2}^{\lambda_1}\ln(\boldsymbol{R}/\boldsymbol{R}_0)d(1/\lambda)$, where λ denotes the wavelength of the incident light and the band strength A is obtained in experiments, where η is independently determined. However, this calculation is not applicable to a reflectance measurement because it is based on the assumption that the optical depth, $-\ln(\boldsymbol{R}/\boldsymbol{R}_0)$, is proportional to η, in accordance with the Beer-Lambert law. Because of the strong effect of optical interference between light reflected from the film and substrate surfaces on the reflectance of the film, Beer's law cannot be used in reflectance, as we recently demonstrated in thin water ice films.[25]

RESULTS AND DISCUSSION

The generation of ozone from solid O_2 is confirmed both by the appearance of the Hartley band in the ultraviolet and the ν_3 and $\nu_1+\nu_3$ bands in the infrared. In Fig. 2 we plot the UV-visible and infrared reflectance of O_2 films near the Hartley and ν_3 bands before and after irradiation with a fluence of

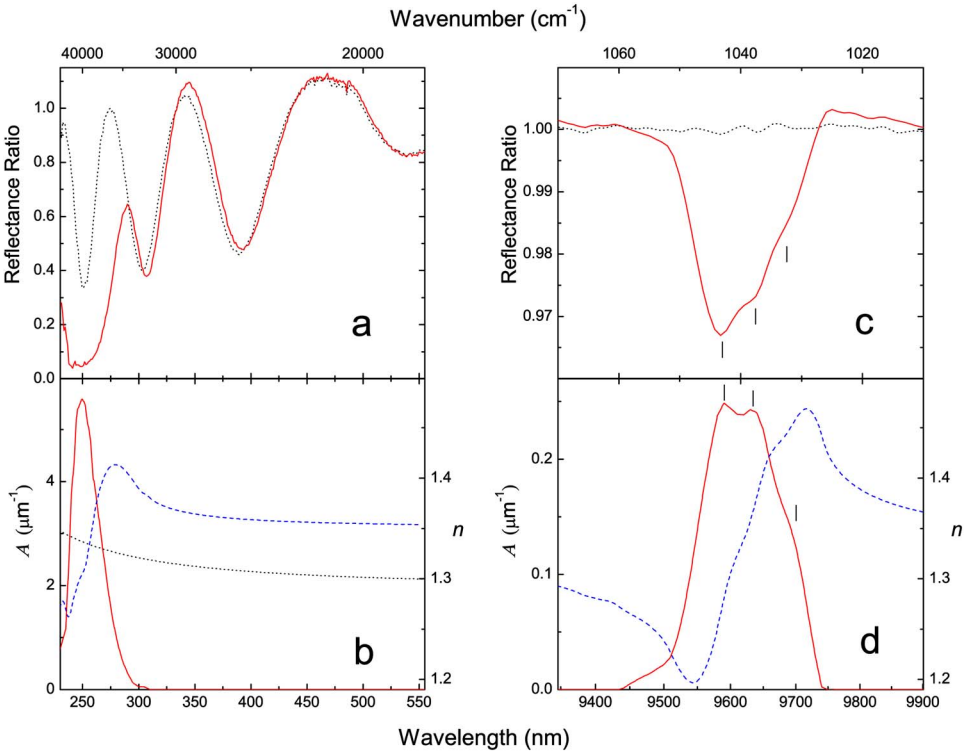

FIG. 2. Changes in the optical properties of an oxygen film with irradiation by 3×10^{14} H^+/cm^2 at 100 keV. (a) The UV-visible reflectance of a 490 nm film before (black dotted line) and after (red line) irradiation. (b) The real part n of the refraction index before irradiation (black dotted line), and the index (dashed blue line) and absorbance A (solid red line) of the same film after irradiation (A is undetectable before irradiation). (c) The reflectance of a 318 nm film near the ν_3 absorption band of ozone before (black dotted line) and after (red line) irradiation. (d) n (dashed blue line) and A (solid red line) of the film of (c) after irradiation. The vertical marks in (c) and (d) indicate the positions of the 1031, 1038, and 1042 cm^{-1} structures mentioned in the text.

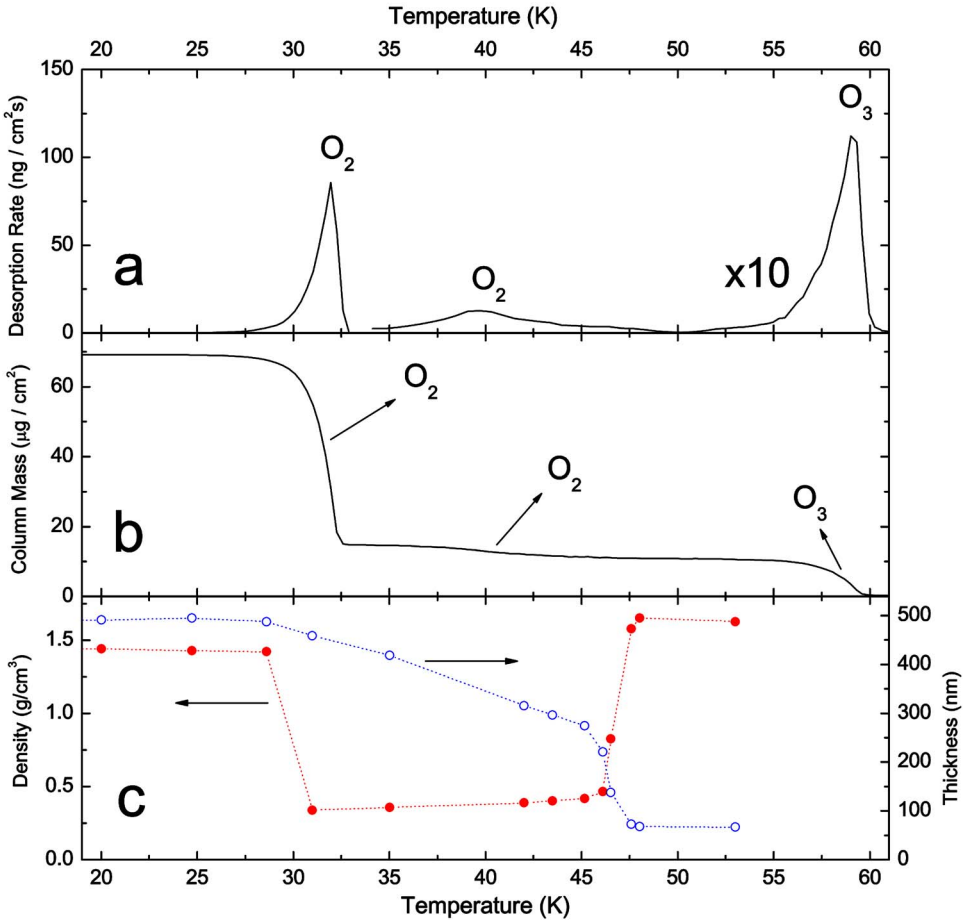

FIG. 3. Evolution of the irradiated 490 nm thick O_2 film of Figs. 2(a) and 2(b) during warming, (a) desorption rate, (b) mass per unit area, and (c) thickness (○) and mass density (●).

3×10^{14} H^+/cm^2, which is sufficient to saturate the concentration of O_3.[4,5] The UV-visible reflectance shows oscillations with maxima and minima corresponding to wavelengths of constructive and destructive interferences in the film, but after irradiation, the Hartley band of ozone is superimposed on the interference, lowering the reflectance below ~300 nm [Fig. 2(a)]. Fitting Eq. (11) to the spectra, we obtain ~490±5 and ~318±5 nm for the thicknesses of films shown in Figs. 2(a) and 2(c), respectively, and the corresponding A and n are shown in Figs. 2(b) and 2(d). A calculation from A and n at the maximum of the Hartley band using Eq. (10) yields $\eta=(2.3\pm0.3)\times10^{17}$ O_3/cm^2 in the 490 nm film, which corresponds to an O_3 concentration of 19±3%. This value is much higher than our previously reported value of 1% (Ref. 4) from measurements of proton irradiated 1:1 O_2:H_2O mixture containing aggregates of solid O_2. A possible explanation for the discrepancy is the production of H atoms in the irradiated mixture, which could scavenge the radiolytic O atoms, thus hindering the formation of O_3 in the aggregates. We point out that the O_3 concentration produced by irradiation of pure O_2 is consistent with the presence of a single broad ν_3 absorption band in the infrared spectrum of irradiated O_2 rather than the isolated absorption peaks seen at lower concentrations.[15] The small structures at ~1031, ~1038, and ~1043 cm^{-1} [Fig. 2(c)] are similar to those detected in experiments with 5 keV electrons.[17]

Films containing O_3 released gas in three stages when warmed (Fig. 3), beginning with evaporation of most of the O_2 at ~30–32 K, which left a residue of ~35% O_2 and 65% O_3. This desorption was followed by a more gradual O_2 release at ~35–46 K, and then the loss of the remaining pure O_3 near ~57–60 K. We attribute the first two desorption peaks at 30–32 and 35–46 K to O_2 on the basis of previous mass spectrometry measurements[5] that do not show desorption of O_3 in this temperature range. Evidence that the solid which desorbs at ~60 K is pure O_3 is provided by Fig. 4, where we have plotted the natural logarithm of the rate of desorption of the inverse of temperature. From the slope of the data, we calculate a sublimation energy of 0.196±0.001 eV (about twice that of solid O_2) in close agreement with the value of 0.203 eV previously measured for solid ozone in the range of 65–90 K.[27]

As shown in Fig. 5, each desorption step is accompanied by drastic changes in the UV-visible reflectance. At 33 K, during the first desorption of O_2, while the mass of the film decreased by 79%, the UV reflectance still showed a minimum at the Hartley band, signaling that most of the ozone remains on the substrate. Moreover, two interference maxima were still present above ~300 nm, but the amplitude of the interference oscillations was less than half of that before O_2 desorption, suggesting a reduction in the index of refraction of the film rather than the thickness.[28] This analysis is confirmed by a fit of Eq. (11) to the reflectance spectrum, which yields a thickness of 460 nm, close to the original thickness of 490 nm. Thus, in spite of the loss of 79% of the mass of the film, the thickness drops by only 6%, resulting in a drastic reduction in density from 1.42 to 0.34 g/cm^3.

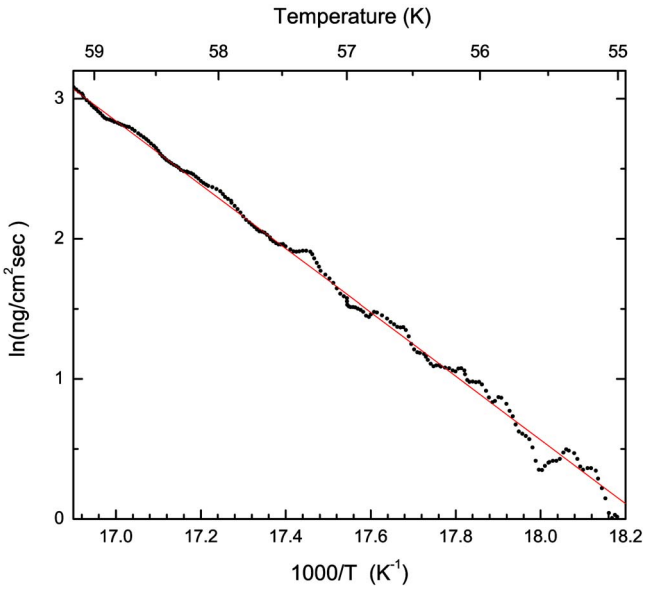

FIG. 4. Arrhenius plot of the desorption rate measured by the microbalance below 60 K of an irradiated O_2 film. The straight line is a fit to the data; its slope times Boltzmann's constant gives a sublimation energy of 0.196±0.001 eV.

As the remaining O_2 desorbed by warming from 35 to 46 K, there was a gradual decrease in thickness to 221 nm, and the density rose to 0.46 g/cm^3, as shown in Fig. 3(c). Then, just after O_2 desorption completes at ~46 K, the thickness dropped sharply to 68 nm, with a corresponding rise in density to 1.65 g/cm^3, a value close to those previously measured for liquid and solid ozone.[29,30] The increase in ozone density drastically alters the interference observed in the UV-visible reflectance spectrum, producing two deep minima at ~465 and ~235 nm in the film at 50 K (Fig. 5) due, respectively, to the destructive interference and to the

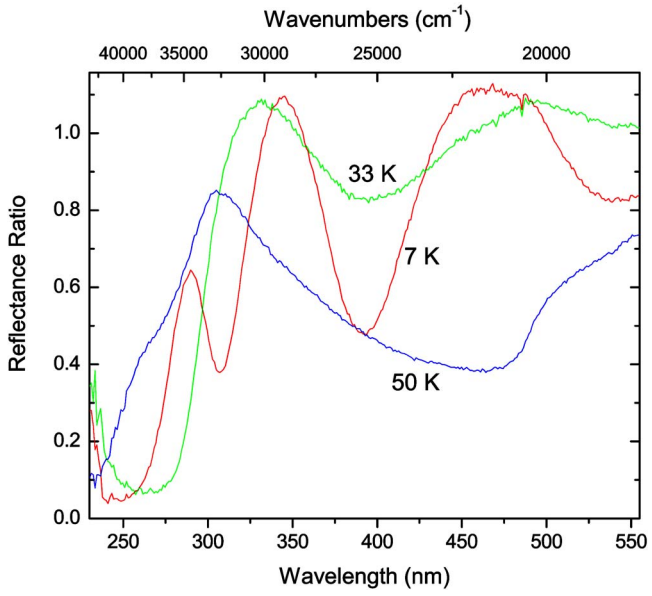

FIG. 5. The UV-visible reflectance of the O_2 film of Fig. 3 just after irradiation at 7 K (red) and during warming at 33 (green) and 50 K (blue). The spectral shape is determined by interference oscillations and the Hartley absorption near 250 nm.

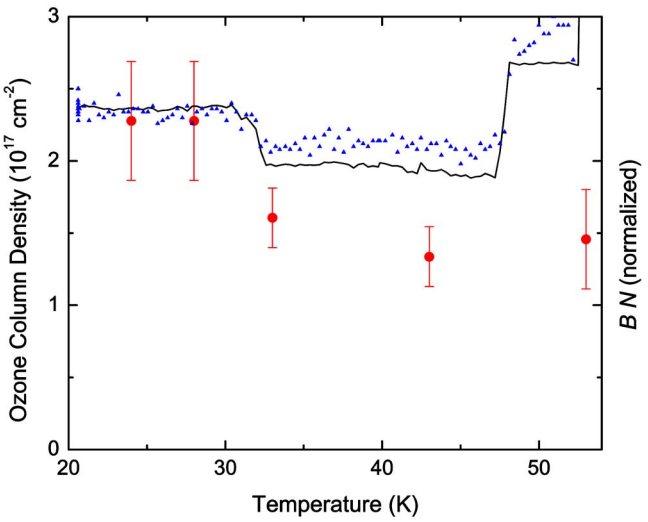

FIG. 6. The O_3 column density calculated using Eq. (10) from the Hartley band for the film of Fig. 5 during warming (●). Also shown is *BN*, the integral of the absorbance across the ν_3 (solid line) and $\nu_1+\nu_3$ (blue triangles) bands of ozone during warming of the 318 nm thick film of Figs. 2(c) and 2(d). Each integral is normalized to the column density scale for comparison purposes. The increase in the ν_3 and $\nu_1+\nu_3$ bands above 45 K is due to changes in band strengths during densification and crystallization of the ozone.

Hartley band of ozone (blueshifted because it is superimposed onto a nearby interference maximum). We have demonstrated the irreversibility of the density increase in separate experiments by cooling this high density ozone back below 46 K (as low as 7 K). The solid retained a high density irrespective of the temperature to which it was cooled, thus demonstrating that the low density ozone is a metastable phase.

As shown in Fig. 6, the column density of ozone declines by ~30% during the first O_2 desorption peak at 32 K. As mentioned earlier, mass spectrometry measurements indicate that ozone does not desorb at these temperatures, indicating that some O_3 is lost by another mechanism. A possible process is the following reaction involving radiolytic O atoms left over from irradiation at 7 K, which have not reacted with O_2:

$$O + O + O_3 \rightarrow O + 2O_2, \tag{12}$$

with the product O_2 simultaneously desorbing from the film. We point out that the integrated areas of the ν_3 and $\nu_1+\nu_3$ infrared bands to not evolve during warming in proportion to the column density as calculated from the Hartley band but instead show conflicting behavior, with the $\nu_1+\nu_3$ band not changing and the ν_3 band area increasing (Fig. 7). Bennett and Kaiser[17] also noted an enhancement in the ν_3 band depth at ~35 K when warming a solid O_2 film irradiated with 5 keV electrons, concluding that an additional ozone was being produced. However, to take due account of optical interference (rather than assuming Beer's law), we use the integral of the absorbance *A* rather that the integral of the optical depth. We find that the integrals for both bands are consistent with the loss of O_3 obtained from the Hartley band (Fig. 6). Normalizing to the density N_{O_3} of ozone yields the band strength,

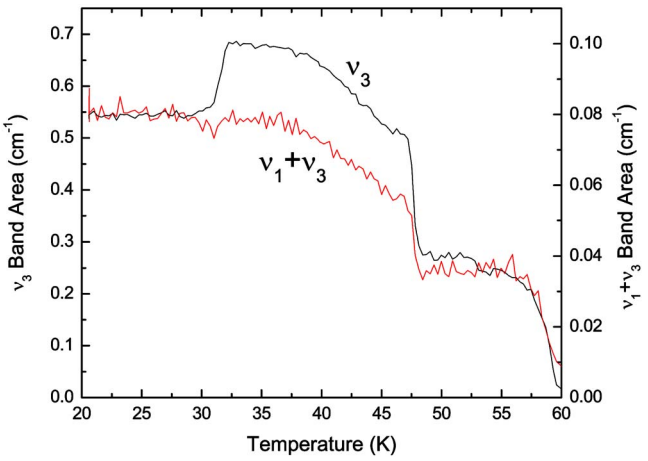

FIG. 7. The integrated area (i.e., in optical depth) of the ν_3 and $\nu_1+\nu_3$ absorption bands of ozone during warming of the 318 nm thick film of Figs. 2(c) and 2(d).

$$B = \frac{1}{N_{O_3}} \int A(\lambda) d(1/\lambda), \tag{13}$$

where $N_{O_3}=h/z$. We give the band strengths in Table I, but warn that these values cannot be used to interpret reflectance experiments unless interference is first taken into account.[25] The band strength for both modes systematically increases with the density due to the enhancement of polarizability induced by neighboring molecules.

As shown in Fig. 8 for an initially 318 nm film, the ν_3 band evolves in several steps when the samples are warmed, beginning with a slight broadening after the initial 30–32 K O_2 desorption. The band changed little until the temperature reached ~47 K, when it narrowed dramatically and shifted to ~1050 cm^{-1}. Then at ~53 K, the temperature where ozone is thought to crystallize,[31] the band deepened and shifted to ~1053 cm^{-1}. In interpreting these changes, we must consider that the density is drastically modified as the film is warmed, with corresponding changes in film thickness and index of refraction that induce spectral distortions due to changing optical interference. A comparison of $A(\lambda)$ [Fig. 9(a)] with the optical depth spectra reveals a distortion sufficiently intense after densification of the low density O_3 that $-\ln(\boldsymbol{R}/\boldsymbol{R}_0)$ does not accurately portray the shape of the ν_3 band. The difference between $A(\lambda)$ and the optical depth is even more remarkable after crystallization of the ozone at ~53 K, with $-\ln(\boldsymbol{R}/\boldsymbol{R}_0)$ showing a narrow peak at 1053 cm^{-1} (and a small peak at 1029 cm^{-1}) in spite of the broad band peaked at 1031 cm^{-1} in $A(\lambda)$. In fact, the appearance of two peaks in the optical depth spectra (Fig. 8) is an

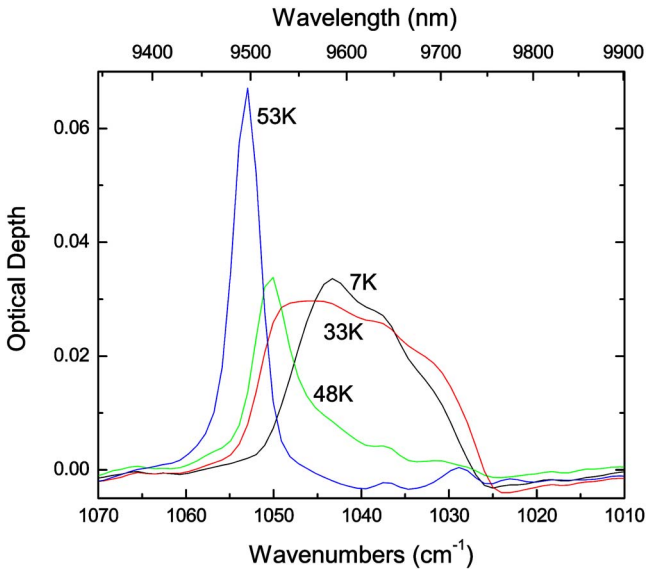

FIG. 8. The optical depth near the ν_3 absorption band of ozone during warming of the 318 nm thick film of Figs. 2(c) and 2(d). The corresponding $A(\lambda)$ and $n(\lambda)$ are given in Fig. 9.

optical interference effect produced by the drastic change in n across the crystalline ν_3 band [Fig. 9(b)], not unlike the example of Fig. 1.

While during O_3 densification at ~47 K the maximum of $A(\lambda)$ shifts from 1043 to 1027 cm^{-1}, we notice in Fig. 10 only a minor change in the molecular polarizability [calculated from Eq. (9)], with the imaginary component of α_{O_3} responsible for absorption retaining a broadly shaped profile peaked at 1043 cm^{-1}. The independence of the polarizability and the density can be understood from the relationship of α to the polarizing field E acting on a molecule, which can be expressed in terms of the dipole moment μ induced in that molecule as follows:

$$\alpha = \mu/E. \tag{14}$$

Unlike A and n, α is insensitive to the enhancement of the polarizing field by the polarization of the neighboring molecules because μ is normalized to E in Eq. (14). Hence, the polarizability is relatively unaffected by the increased proximity between molecules after the O_3 density increase, whereas A and n undergo significant distortion resulting from their nonlinear relationship to N_{O_3} [Eqs. (3) and (9)]. The lack of change in polarizability also suggests that the ozone retains an amorphous molecular structure during densification, especially given the drastic change in α_{O_3} caused by crystallization at 53 K. As shown in Fig. 10(a), the imaginary part of $\alpha_{O_3}(\lambda)$ exhibits a narrow symmetrical peak cen-

TABLE I. Band strengths for the ν_3 and $\nu_1+\nu_3$ O_3 infrared bands for ozone in different conditions.

ν_3 (10^{-17} cm/molecule)	$\nu_1+\nu_3$ (10^{-17} cm/molecule)	Ozone structure
1.4	0.10	Diluted in O_2 (7 K)
1.5	0.14	Low density amorphous (33 K)
2.2	0.18	High density amorphous (48 K)
4.5	0.32	Crystalline (53 K)

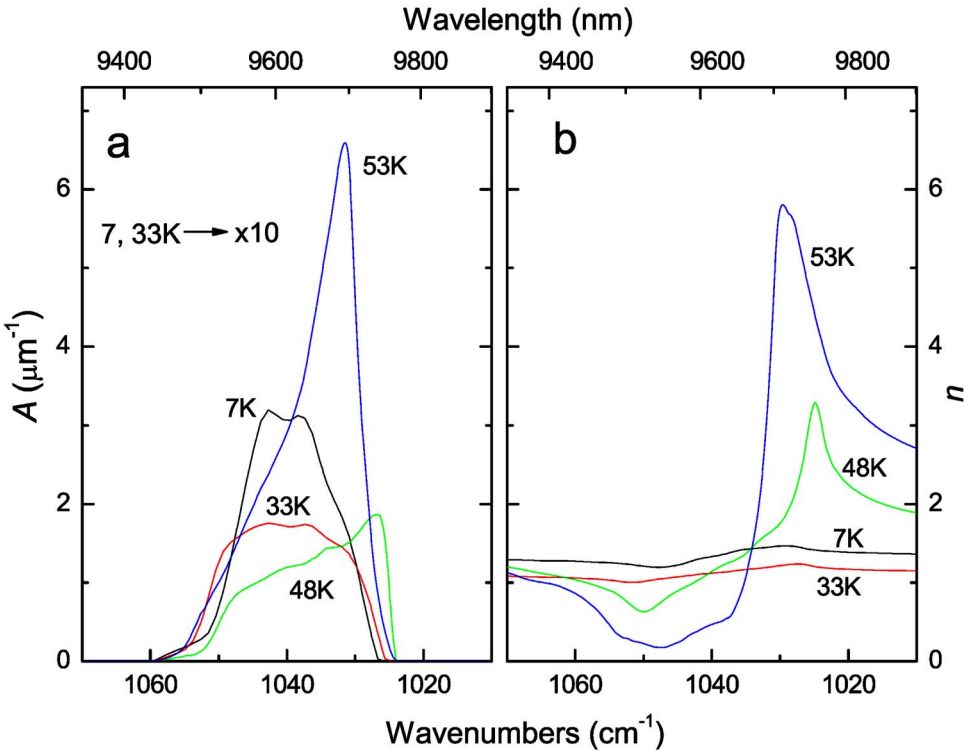

FIG. 9. The (a) absorbance and (b) refraction index (real part) during warming of an irradiated O_2 film obtained by a fit of Eq. (11) to the spectra of Fig. 8. Temperatures shown are 7 K (black line), 33 K (red line), 48 K (green line), and 53 K (blue line). The absorbance at 7 and 33 K is multiplied by 10 for ease of comparison.

tered at 1046.6 cm^{-1} after crystallization. We note the contrast with $A(\lambda)$, which is still distorted by the effect of high density, showing a broad asymmetrical profile peaked at 1031.5 cm^{-1}.

Finally, we point out that Eq. (11) predicts a satellite band close to those reported by Chaabouni *et al.*[31] near ~1050 cm^{-1} (Fig. 11) when the $A(\lambda)$ and $n(\lambda)$ for crystalline O_3 are used to calculate the reflectance of an ozone film at the incidence angle and thickness range used by these authors ($\theta_0=5°$, $z<500$ nm), as shown in Fig. 11(a). Our results also anticipate those of Chaabouni *et al.* in the case of an O_3:Ar mixture deposited at 20 K from which the Ar was subsequently desorbed [Fig. 11(c)], provided that the solid is assumed to have a density of ~0.84 g/cm^3. Thus, a comparison of our results with the measurements of these authors shows that the solid ozone with a reduced density is formed by warming of a mixture containing O_3 even if the second component is not O_2. In contrast, we have verified in separate experiments that direct deposition of pure O_3 produces a high density ozone even below 47 K. We measure a density

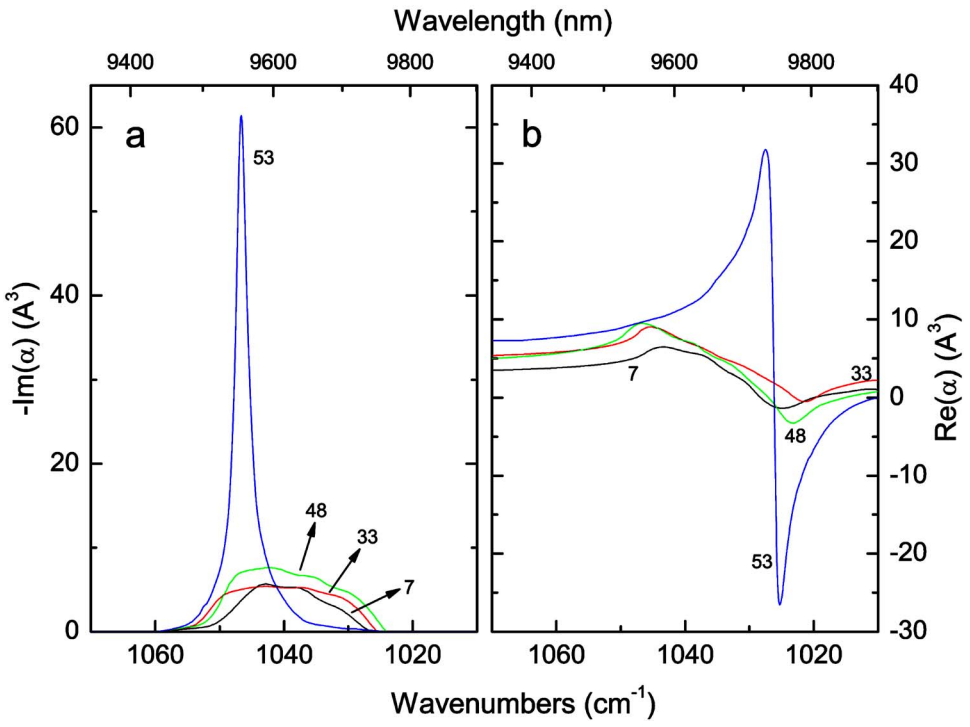

FIG. 10. The (a) imaginary and (b) real parts of the molecular polarizability during warming of an irradiated O_2 film calculated from the $n(\lambda)$ and $A(\lambda)$ given in Fig. 9 using Eq. (9), where $N_{O_2}=(Q-\eta M_{O_2})/zM_{O_3}$ and μ_{O_2} is calculated using Eq. (3) from the refraction index of pure O_2 [Fig. 2(b)] in the long wavelength limit (μ_{O_2} is, for our purposes, taken to be temperature independent). Temperatures shown are 7 K (black), 33 K (red), 48 K (green), and 53 K (blue).

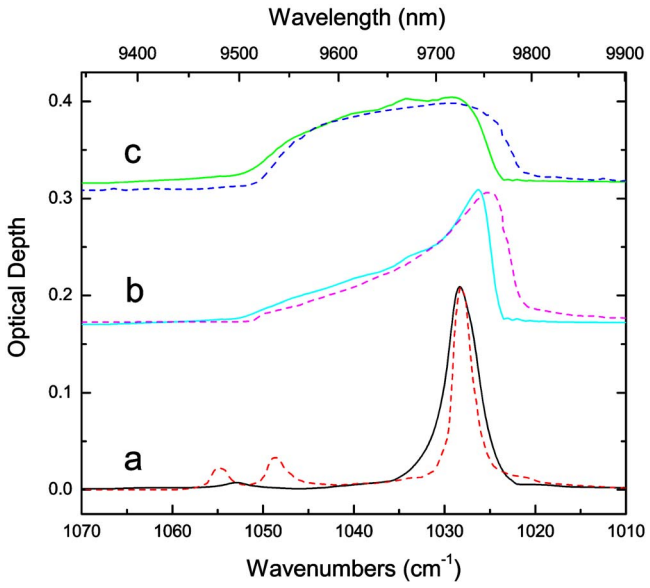

FIG. 11. Dotted lines show the optical depth spectra of solid O_3 near the ν_3 band measured by Chaabouni *et al.* (Ref. 31) for (a) a crystalline ozone film deposited at 55 K, and (b) an ozone film deposited at 30 K with helium as a carrier gas, and (c) an ozone-argon mixture deposited at 20 K from which the argon was desorbed (by warming to 40 K). Solid lines show the optical depth predicted on the basis of our results. We used our measurements of $\alpha_{O_3}(\lambda)$ for crystalline and amorphous ozone to calculate $A(\lambda)$ and $n(\lambda)$ at different densities [using Eq. (11)], then chose the density that gave the best fit of Eq. (11) to the data of Chaabouni *et al.* under their experimental conditions. The densities and film thicknesses for each fit are (a) 1.63 g/cm^3 and 200 nm, (b) 1.43 g/cm^3 and 365 nm, and (c) 0.84 g/cm^3 and 500 nm.

of $\sim$1.65 g/cm^3 with ozone deposition temperatures down to 10 K, which is slightly higher than the density of $\sim$1.42 g/cm^3 suggested by the spectrum of Chaabouni *et al.* for O_3 deposition at 30 K (Fig. 11), a difference that could be related to the use of helium as a carrier gas by these authors.

The creation of a low density residue by desorption of O_2 in our experiments might be compared with the preparation of porous materials such as cryogels, where the more volatile component of a solidified mixture is allowed to sublime in a freeze-drying process, resulting in a highly porous solid (e.g., Ref. 32). Indeed, the phenomenon of porosity in condensed gases is well known in the case of water ice, which forms a microporous solid when vapor is deposited below $\sim$100 K.[33] An important property of porous solids is the high surface area available for gas adsorption (e.g., hundreds of m^2/g), and adsorption measurements have been utilized extensively to characterize the porosity structure of different materials.[34] To check for the existence of a porous structure in our case, we held the temperature of the film at 33 K in one experiment and filled the vacuum chamber with different pressures of O_2 after formation of the low density residue, while measuring the amount of gas adsorbed with the microbalance. Remarkably, we detected negligible gas adsorption ($<10^{15}$ O_2/cm^2) at all pressures below the vapor pressure ($\sim10^{-5}$ Torr at 33 K) of O_2 (O_2 condensed as an overlayer on top of the ozone above this pressure), indicating either that the low density residue is nonporous or that the pores are completely isolated from the external vacuum.

In separate experiments, we lowered the ozone concentration in the film before warming by using irradiation fluences less than 2×10^{14} H^+/cm^2 or by codepositing O_2 and O_3 to produce O_2/O_3 mixtures with low O_3 concentrations (i.e., $<$19%). In the latter case we produced pure ozone in a glass manifold via liquid nitrogen distillation of O_2 gas excited with a Tesla coil. The ozone could then be vapor deposited as a pure solid from a glass doser or deposited simultaneously with O_2 using two dosers to produce O_2/O_3 mixtures of different concentrations. Lowering the ozone concentration merely diminished the thickness of the residue produced on warming without lowering its density below 0.3 g/cm^3, thus demonstrating that the solid exists as a low density phase with a fixed density. Moreover, the stability of this phase is not strongly affected by the O_2 concentration remaining in the residue (35%), since most of the O_2 desorbs below $\sim$46 K during warming, while the remaining ozone only fully compacts at $\sim$47 K [Fig. 3(c)]. Hence, our results show the existence of a low density phase of amorphous ozone. Since a homogeneous, isotropic molecular structure with a density of 0.34 g/cm^3 requires an implausibly high average separation distance of $\sim$6 Å between molecules, we suggest that the ozone exists as a foamlike structure consisting of voids, which are isolated from the outside of the solid. The O_2 initially retained after formation of the low density solid at 33 K could exist as a solid or a gas within such voids. However, the mechanism for the escape of the O_2 and the reason for the sudden collapse of the low density structure at $\sim$47 K require further investigation.

CONCLUSIONS

We have demonstrated the formation of a low density phase of solid ozone by desorption of O_2 from O_2:O_3 mixtures using reflectance spectroscopy and a quartz-crystal microbalance. Coupled with a careful analysis of reflectance spectra, the discovery of a low density phase provides an explanation for the temperature dependence of ozone infrared spectra found in a previous research and helps us to answer questions regarding the shape of the ν_3 absorption band. The results suggest the possibility that the isolated voids are responsible for the low density phase, but further research is needed to characterize the details of the molecular structure and the precise mechanism responsible for the transition of the ozone to a high density state at $\sim$47 K.

ACKNOWLEDGMENT

This research was supported by NASA's Origins of the Solar System and Planetary Atmospheres programs.

[1] K. S. Noll, R. E. Johnson, A. L. Lane, D. L. Domingue, and H. A. Weaver, Science **273**, 341 (1996).
[2] K. S. Noll, T. L. Roush, D. P. Cruikshank, R. E. Johnson, and Y. J. Pendleton, Nature (London) **388**, 45 (1997).
[3] S. Lacombe, F. Cemic, K. Jacobi, M. N. Hedhili, Y. Le Coat, R. Azria, and M. Tronc, Phys. Rev. Lett. **79**, 1146 (1997).
[4] R. A. Baragiola, C. L. Atteberry, D. A. Bahr, and M. M. Jakas, Nucl. Instrum. Methods Phys. Res. B **157**, 233 (1999).
[5] M. Famá, D. A. Bahr, B. D. Teolis, and R. A. Baragiola, Nucl. Instrum. Methods Phys. Res. B **193**, 775 (2002).
[6] B. D. Teolis, M. J. Loeffler, U. Raut, M. Famá, and R. A. Baragiola, Astrophys. J. **644**, L141 (2006).
[7] A. E. Dessler, *The Chemistry and Physics of Stratospheric Ozone* (Academic, New York, 2000).

[8] L. Brewer and J. L.-F. Wang, J. Chem. Phys. **56**, 759 (1972).
[9] L. Andrews and R. C. Spiker, Jr., J. Phys. Chem. **76**, 3208 (1972).
[10] P. Brosset, R. Dahoo, B. Gauthier-Roy, and L. Abouaf-Marguin, Chem. Phys. **172**, 315 (1993).
[11] A. Lakhlifi, C. Girardet, R. Dahoo, P. Brosset, B. Gauthier-Roy, and L. Abouaf-Marguin, Chem. Phys. **177**, 31 (1993).
[12] P. Ehrenfreund, M. Burgdorf, L. d'Hendecourt, and J. M. Greenberg, Adv. Space Res. **13**, 465 (1993).
[13] H. Frei, L. Fredin, and G. C. Pimentel, J. Chem. Phys. **74**, 397 (1981).
[14] M. Bahou, L. Schriver-Mazzuoli, and A. Schriver, J. Chem. Phys. **114**, 4045 (2001).
[15] L. Schriver-Mazzuoli, A. de Saxcé, C. Lugez, C. Camy-Peyret, and A. Schriver, J. Chem. Phys. **102**, 690 (1995).
[16] M. J. Dyer, C. G. Bressler, and R. A. Copeland, Chem. Phys. Lett. **266**, 548 (1997).
[17] J. Bennett and R. I. Kaiser, Astrophys. J. **635**, 1362 (2005).
[18] N. J. Mason, J. M. Gingell, J. A. Davies, H. Zhao, I. C. Walker, and M. R. F. Siggel, J. Phys. B **29**, 3075 (1996).
[19] M. Born and E. Wolf, *Principles of Optics*, 7th ed. (Cambridge University Press, Cambridge, 1999), pp. 46–47.
[20] O. S. Heavens, *Optical Properties of Thin Solid Films* (Butterworths, London, 1955).
[21] F. Stern, in *Solid State Physics*, edited by F. Seitz and D. Turnbull (Academic Press, New York/London, 1963), Vol. 15, p. 324.
[22] W. Hagen, A. G. G. M. Tielens, and J. M. Greenberg, Chem. Phys. **56**, 367 (1981).
[23] D. M. Hudgins, S. A. Sandford, L. J. Allamandola, and G. G. M. Tielens, Astrophys. J., Suppl. Ser. **86**, 713 (1993).
[24] G. A. Baratta and M. E. Palumbo, J. Opt. Soc. Am. A **15**, 735 (1998).
[25] B. D. Teolis, M. J. Loeffler, U. Raut, M. Famá, and R. A. Baragiola, Icarus (in press).
[26] D. W. Berreman, Phys. Rev. **130**, 2193 (1963).
[27] D. Hanson and K. Mauersberger, J. Chem. Phys. **85**, 4669 (1986).
[28] M. S. Westley, G. A. Baratta, and R. A. Baragiola, J. Chem. Phys. **108**, 3321 (1998).
[29] A. G. Streng and A. V. Grosse, J. Am. Chem. Soc. **81**, 805 (1959).
[30] R. I. Brabets and J. M. McDonough, J. Chem. Phys. **27**, 880 (1957).
[31] H. Chaabouni, L. Schriver-Mazzuoli, and A. Schriver, J. Phys. Chem. A **104**, 6962 (2000).
[32] H. Tamon, H. Ishizaka, T. Yamamoto, and T. Suzuki, Carbon **37**, 2049 (1999).
[33] K. P. Stevenson, G. A. Kimmel, Z. Dohnalek, R. S. Smith, and B. D. Kay, Science **283**, 1505 (1999).
[34] F. Rouquerol, J. Rouquerol, and K. Sing, *Adsorption by Powders and Porous Solids: Principles, Methodology and Applications* (Academic, San Diego, 1999).